ARTICLE

Tunable fluorescence emission for multi-color light-emitting diodes and voice-activated intelligent lighting applications

Received 00th January 20xx,
Accepted 00th January 20xx

DOI: 10.1039/x0xx00000x

Yiwei Liu,[a] Yuanwei Wang,[b] Xinyi Song,[a] Xiaohui Wang,[a] Haoxian Zhu,[a] Juchang Zhang,[a] Jie Bai,[a] Carl Redshaw,[c] Xin-Long Ni,[d] Xing Feng,*[ae] Dong Wang[b] and Ben Zhong Tang*[bf]

With the development of the microelectronics technology, personalized intelligent lighting and lighting control systems have been widely utilized in smart buildings to save energy, facilitate people's lives, as well as decorate our community environment. This article presents four bipolar molecules (**1**-**4**) with bright color-tunable emission from blue (446 nm) to red (637 nm) light, which were designed and synthesized via constructing a pull-push system. Moreover, these highly thermally stable with tunable fluorescence emission molecules were used as a high-efficient emitter for fabricating stable RGB LED devices with a considerable color rendering index (CRI). Furthermore, we designed an electrocircuit system to control the green, red and yellow LED devices using an "ON" and "OFF" switch via voice-activated microelectronics technology. Thus, this study not only provides a molecular strategy to construct tunable-emission materials for multi-color LED device applications, but also offers an efficient example for combining organic synthesis with electronic devices to realize a personalized intelligent lighting and light control system via microelectronics technology.

Introduction

The development of information technology, the internet of things (IoT) and the fifth-generation (5G) wireless networks have opened up many new research avenues and have led to a revolution in technological innovation and human daily life.[1] The smart house/city is one of the important embodiments of IoT,[2] and involves various electronic equipment, such as intelligent lighting systems,[3, 4] audio video devices and security systems etc.[5] Among them, voice-activated intelligent lighting can translate the voice commands, and realize control of the light.

Currently, light-emitting diodes (LEDs) and organic light-emitting diodes (OLEDs) have been used as popular lighting system in smart houses/cities,[6] and organic fluorescent materials with color-tunable emission are an essential component for potential applications of OLEDs,[7] biological sensing, bioimaging,[8, 9] anti-counterfeiting and so on.[10] Compared to inorganic phosphors, organic materials possess exact molecular structures with molecular skeletons that are readily modified, which is beneficial for accessing an incredible variety of fluorescence materials with fantastic photophysical properties, such as stable luminescent radicals,[11] color-tunable emission, as well as singlet fission,[12] room-temperature-phosphorescence,[13] and so on.[14, 15] Thus, much effort has been devoted to the development of novel organic fluorescent materials to realize high-tech organic electronic devices with advanced applications.

Moreover, many strategies have been explored to construct tunable fluorescent emission organic molecules for multi-color emitters, as well as white-light emitters, such as ratio responsive luminescent materials,[16] fluorescence-phosphorescence hybrid dual emission materials,[17, 18] dual emission materials with fluorescence and thermal activation delayed fluorescence (TADF) characteristics etc.[19] For instance, Li and coworkers reported a single-molecule white-light emitting hydrogel which exhibited multicolor emission due to its high sensitivity to H^+ and temperature.[20] Chi *et al*. found that the formation of intermolecular C-H···O hydrogen bonds in crystals of an asymmetrical diphenylketone derivative, play a significant role in balancing the intramolecular charge transfer and intermolecular charge transfer, which led to persistent dual-emission properties.[21] The above-mentioned examples are single-component systems with color-tunable emission. However, luminescent materials with stable red, green or blue color exhibit unique optical properties, such as stronger

[a.] *Guangdong Provincial Key Laboratory of Information Photonics Technology. School of Material and Energy, Guangdong University of Technology, Guangzhou 510006, P. R. China.*
[b.] *Center for AIE Research, Shenzhen Key Laboratory of Polymer Science and Technology, Guangdong Research Center for Interfacial Engineering of Functional Materials, College of Materials Science and Engineering, Shenzhen University, Shenzhen 518060, P. R. China.*
[c.] *Department of Chemistry, University of Hull, Cottingham Road, Hull, Yorkshire HU6.*
[d.] *Key Laboratory of the Assembly and Application of Organic Functional Molecules of Hunan Province, Hunan Normal University, Changsha 410081, P. R. China.*
[e.] *Guangdong Provincial Key Laboratory of Luminescence from Molecular Aggregates (South China University of Technology), Guangzhou 510640, P. R. China.*
[f.] *Shenzhen Institute of Aggregate Science and Technology, School of Science and Engineering, The Chinese University of Hong Kong, Shenzhen, 2001 Longxiang Boulevard, Longgang District, Shenzhen City, Guangdong 518172, China.*
[g.] *Electronic Supplementary Information (ESI) available: the $^1H/^{13}C$ NMR and HRMS spectra of the new compounds; absorption and fluorescence spectra. (PDF). CCDC 2119848.*

emission intensity, non-dependent-microenvironmental emission properties, and show great application in OLEDs.[22]

On the other hand, light-emitting diodes (LEDs) are one of the most important electronic devices for displays and lighting applications, as well as landscaping our community. Combining electronic information technology with advanced LEDs, provides intelligent devices that are an important personal item in our daily lives. Herein, a set of organic fluorescent molecules are designed for fabricating high-efficiencies RGB light LED and a yellow light LED using a UV InGaN chip as the excitation source. Thus, the focus here is on the preparation of color-tunable organic fluorescence molecules formed by combining a components such as a pyrene core and benzothiadiazole with triphenylamine units, and these subsequently were used for the fabrication of blue, green and red LEDs. Moreover, we have designed an efficient personalized intelligent lighting device for controlling the corresponding LED by voice-activated microelectronics technology.

Results and discussion

Molecular design, synthesis and characterization

To achieve a wide color-tunable emission from blue to red color, one molecular design strategy is to construct an efficient electron push-pull system, which can efficiently regulate the molecular energy gap by incorporating suitable electron-donating (D) and electron-withdrawing (A) groups, leading to an expected light emission.

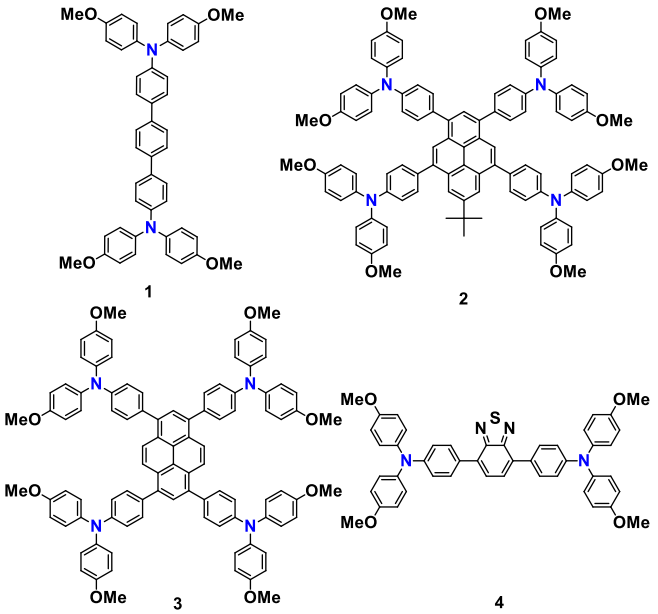

Fig. 1 The designed color-tunable emission molecules **1**-**4**.

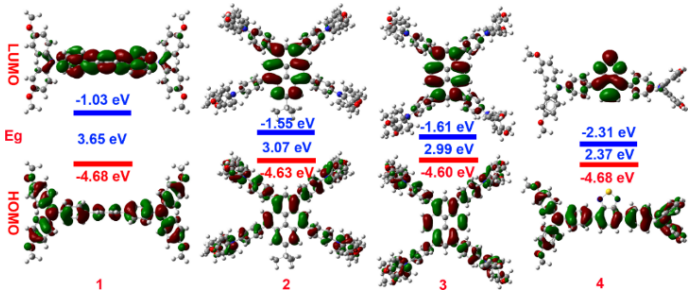

Fig. 2 Optimized molecular orbital plots (B3LYP/6-311G(d,p)) of molecules **1**-**4**; the blue and red in the molecular configuration represent electron density.

Herein, we selected the triphenylamine unit as the electron-donating unit, which was combined with phenyl or an electron-acceptor such as pyrenyl or benzothiadiazole group as bridge units to form the bipolar molecules **1**-**4**, respectively. It is worth noting that pyrene may act an electron-withdrawing group in molecules **2** and **3**, due to its sensitivity to the micro-environment of the complete molecular framework.[23-25]

Firstly, the geometries of four model molecules were optimized by density functional theory (DFT) methods using the B3LYP/6-311 G (d,p) function. As expected, the electron clouds in the HOMO of the bipolar molecules **1**-**4** are delocalized over the whole molecular skeleton via π-conjugation, and the LUMO are mainly located at the terphenyl, pyrene and benzothiadiazole units, respectively, indicated that the components act as an electron-accepting group. Interestingly, the HOMO energy levels of molecules **1**-**4** show a slight change over the range from -4.60 to -4.68 eV, but the LUMO levels increased from -2.31 to -1.03 eV, leading to a decreased HOMO-LUMO energy gap (E_g) from 3.65 to 2.37 eV (Table 2). Clearly, the electron-withdrawing group plays a crucial role in adjusting the molecular energy gap via enhancing the LUMO energy level. According to the DFT calculation results, it is speculated that the designed molecules **1**-**4** have potential as color-tunable emission materials for full-color display applications.

The designed molecules **1**-**4** were synthesized by classical Pd-catalyzed coupling reactions between (4-(bis(4-methoxyphenyl)amino)phenyl)boronic acid with the corresponding bromides in considerable yield and the detailed synthetic route is listed in Scheme S1. The target compounds **1**-**4** were soluble in common organic solvents, such as CH_2Cl_2, $CHCl_3$, dimethyl sulfoxide (DMSO) and tetrahydrofuran (THF), and their identities were further confirmed by $^1H/^{13}C$ NMR spectroscopy, high resolution mass spectrometry (HRMS) (Figs. S1-S10 in the supporting information), as well as thermogravimetric analysis (TGA). All compounds exhibited good thermal stability with 5% weight loss temperature (decomposition temperature, T_d) over the range 419-433 °C. Differently, the TGA results indicated that the compounds **1** and **4** contained amounts of solvent molecules (e.g. hexane or CH_2Cl_2 molecules) in their crystalline form, leading to a 12-18% weight loss at less than 150 °C (Fig. S11).

Table 1. The photophysical properties of **1**-**4**

Comd.	$\Lambda_{max\ abs}$ [a] nm/(M^{-1}/cm^{-1})	λ_{maxPL} (nm)	Φ_f	τ (ns) Sol./film	Td[b]
1	300 (34000) 361 (59800)	446 (THF) 449 (film) 470 (powder)	0.45 (THF) 0.09 (film)	0.47 / 1.98	419
2	302 (59000) 370 (32000) 410 (27800)	499 (THF) 497 (film) 502 (powder)	0.56 (THF) 0.11 (film)	1.47 / 3.63	431
3	302 (79000) 372 (38700) 424 (43700)	500 (THF) 506 (film) 540 (powder)	0.61 (THF) 0.13 (film)	1.48 / 2.96	431
4	321 (42800) 482 (18500)	637 (THF) 647 (film) 661 (crystal)	0.20 (THF) 0.10 (film)	4.24 / 2.92	433

[a] Maximum absorption wavelength measured in THF at room temperature. [b] Decomposition temperature (T_d) obtained from thermogravimetric analysis (TGA).

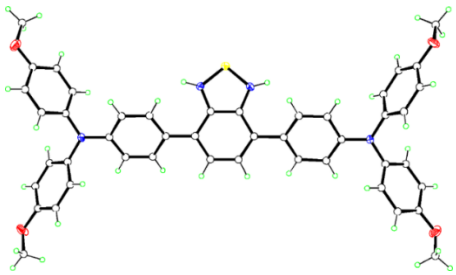

Fig. 3 ORTEP drawing of compound **4**.

A suitable crystal of **4** for single crystal X-ray diffraction analysis was cultivated from a mixture of CH_2Cl_2 and hexane by the slow solvent evaporation method. It crystallized in the monoclinic space group P 1 21/n 1 (Table S1). As shown in Fig. 3, the molecules are non-planar and the dihedral angle between the benzothiadiazole unit and one phenyl of the triphenylamine unit is 35.63°. The neighboring molecules are connected to each other by several C-H···π interactions and hydrogen bonds (C-H···O), but no π-π stacking interactions were observed in the molecular packing.

Photophysical properties

The photophysical properties of the four molecules **1**-**4** were investigated by UV-vis absorption spectra in dilute THF. As shown in Fig. 4A, the absorption spectra of compound **1** exhibits two intense peaks at 300 nm and 361 nm with molar extinction coefficients (ε) in the range between 34000 and 59800 M^{-1} cm^{-1}. The longer wavelength absorption band is consistent with the π-π* electron transition of the whole molecular skeleton of **1**, and the shorter wavelength absorption band is attributed to the electronic transition of the individual aromatic units, respectively. As the electro-withdrawing ability increased following the order of phenyl < pyrenyl < benzothiadiazole in compounds **1**-**4**, this led to a stronger electronic pull-push ability, and the longer wavelength absorption peak was red-shifted from 361 to 482 nm, with a deceased ε from 59800 M^{-1} cm^{-1} to 18500 M^{-1} cm^{-1}, while the ε for the shorter wavelength absorption peak was enhanced from 34000 to 79000 M^{-1} cm^{-1} (Table 1). The high ε values of the short-wavelength for compounds **1**-**4** may due to the presence of overlapping higher energy electronic transitions often obscured by the vibrational bands, leading to a higher molar extinction coefficient.[26] The solvatochromic effect results of compounds **1**-**4** showed that the solvent polarity has a limited effect on the absorption behavior (Figs. S12-S15), indicating that the ground state of each structure is independent on the solvent polarity.[27] In addition, the longer wavelength absorption peak of **3** has red-shifted by *ca*. 14 nm compared to **2**, because the substituents at the 1,3,6,8-positions of the pyrene core have stronger electronic communication than those at the 1,3,5,9-positions, leading to a red-shifted absorption band.[28]

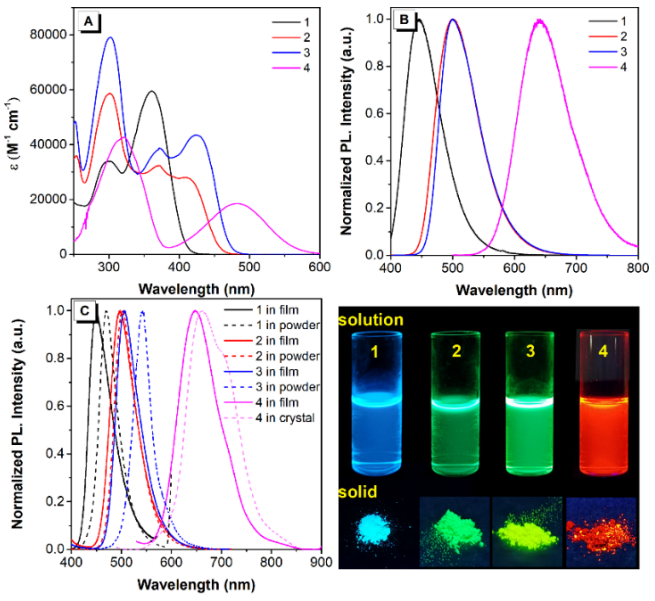

Fig. 4 (A) UV-vis spectra of compounds; (B) fluorescence spectra of compounds **1**-**4** in THF; (C) in the solid state at RT; (D) Fluorescence photographs of **1**-**4** in THF and in the solid state, respectively.

Upon excitation, the four compounds **1**-**4** emit bright and stable the three-primary colors with emission from blue to red

light. The maximum emission peak was located at 446 nm for **1**, 499 nm for **2**, 500 nm for **3** and 637 nm for **4**, respectively. The emission of the compounds **1**-**4** in thin film is red-shifted to the entire visible region over the range from pure blue to red with maximum emission peak at 449 nm (**1**), 497 nm (**2**) and 506 nm (**3**) and 647 nm (**4**), respectively. On the other hand, although we failed to cultivate suitable crystals for X-ray diffraction analysis in mixtures of CH_2Cl_2 and hexane, the achieved powders **1**, **3** and crystal **4** still exhibited a slight red-shift (*ca*. 24-40 nm) compared with the luminescence of their thin film state.

This may be attributed to molecular aggregation in the powder/crystal leading to stronger intermolecular interactions.[24, 29] In addition, compounds **1**-**4** in the powder state have increased narrow full width at half maximum (FWHM) with 53 nm, 60 nm, 55 nm and 96 nm in the powder, respectively, compared to in solution and in thin films, indicative of a high color purity RGB emitter. In addition, the compounds **1**-**4** exhibit clear solvatochromic properties (Figs. S12-S15). As the solvent polarity increasing from hexane to DMSO, the maximum of **1**-**4** red-shifted by up to 95 nm (Table S2). The maximum Stokes shift is 117 nm for **1**, 157 nm for **2**, 140 nm for **3** and 192 nm for **4**, respectively. Indicating that all of the compounds are bipolar molecules with a strong pull-push system.

Furthermore, the stability of the compounds **1**-**4** in THF solution (~10^{-5} M) were evaluated by UV light (λ_{ex} = 365 nm) irradiation for 240 mins, and the whole process was traced by UV-vis and PL spectra. As shown in Figs. S16 and S17, as the UV irradiation time extended, the intensity of the key absorption and emission peak of the corresponding compounds slightly enhanced, but no new absorption peak appeared. This indicated that the compounds were very stable in THF solution under UV irradiation.

The redox properties of the compounds **1**-**4** were determined by cyclic voltammetry (CV), using platinum, platinum wire and a Ag/AgCl electrode as working electrode, auxiliary electrode, and reference electrode, respectively. The measurements were performed under a N_2 atmosphere in 0.12 mol/L anhydrous dichloromethane containing tetrabutylammonium hexafluorophosphate as supporting electrolyte. The cyclic voltammograms are shown in Fig. 5 and the related electrochemical data are summarized in Table 2. The compounds **1**, **2** and **4** display a reversible oxidation wave with half-wave potentials ($E_{ox}^{1/2}$) at 0.64 eV, 0.66 eV and 0.47 eV, and an irreversible oxidation wave with peak potential (E_{pc}) at 1.46eV, 1.45eV and 1.29 eV, respectively. Interestingly, compound **3** exhibits four well resolved quasi-reversible oxidation waves with peak potential (E_{pc}) at 0.51 eV, 0.79 eV, 1.21 eV and 1.49 eV, respectively.

Clearly, the blue emitters **1** and **2** have a higher oxidation potential compared to compounds **3** and **4**. Moreover, the strong redox properties of the four compounds **1**-**4** indicated that the produced radical cation can be stabilized by the expanding π-conjugated molecular framework.[30] In addition, compound **4** displays a clear reversible reduction wave with peak potential (E_{pc}) at -1.78 eV, whereas the other systems did not show any reduction wave, indicating that the electron withdrawing benzothiadiazole group not only could contributes to producing the cathodic reductions, but also stabilizes the radical anions.

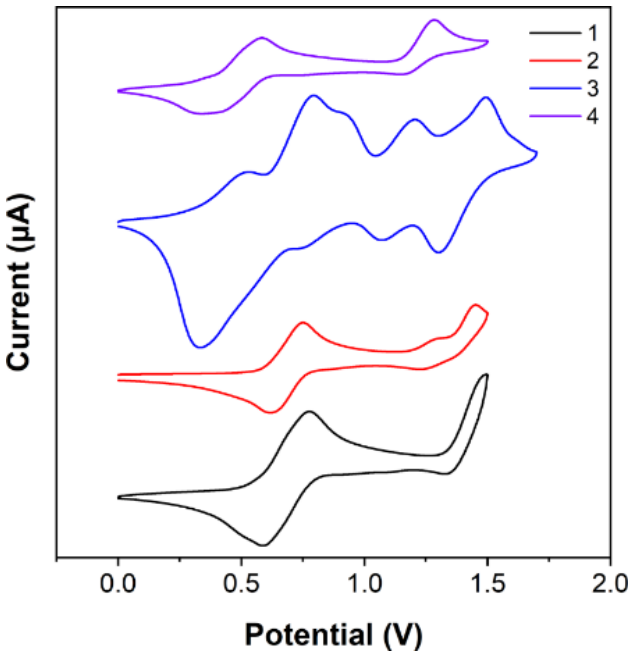

Fig. 5 CV of the compounds **1**-**4** recorded from a CH_2Cl_2 solution on a platinum plate electrode at a scan rate of 100 mV·s^{-1}.

Fabrication of LED devices

In order to test the potential application of the color-tunable organic fluorescent emitters for solid-state lighting, a high-performance RGB LED and a yellow LED with different correlated color temperature (CCT) were fabricated with blue InGaN chips, using compounds **1**-**4** as luminescent materials. The quantum yield of the doped-film with compounds **1**-**4** were in range from 0.47-0.97, respectively. As shown in Fig. 6, under λ_{ex} = 365 nm irradiation, the compounds emit a strong blue, green and red emission with the CIE (Commission Internationale de L'Eclairage 1931) color coordinates of (0.20, 0.19) for b-LED 1, (0.39, 0.54) for g-LED 2, (0.34, 0.60) for g-LED 3 and (0.69, 0.31) for r-LED 4, respectively. Specially, the blue LED has a correlated color temperature of 100000K with considerable color rendering index (CRI) of 70. As the emission color was changed from blue to red, the CCT was decreased from 100000 to 1280 K, indicated that the light color became warmer. It is worthy to note that the g-LED 3 has an extremely luminous efficacy of 6.91 lm/W compared to the others. [31] Since the four color-tunable organic fluorescent emitters **1**-**4** have great thermal stability and air-stable properties, the drive current was increased to higher than 200 mA, and both PL intensity of LED 1 and LED 4 shows a slight decline, while as the working current increased from 20 mA to 300 mA, the LEDs 2 and 3 also exhibit a stable emission and only a minor change of CIE, with an increased emission intensity (Fig. S18). Furthermore, for device 5 was coated with the mixture of blue emitter **1** and red emitter **4** (W1:W4 = 3:7) on the commercial LED chip, and this displayed a broad light

ARTICLE

Table 2 Electrochemical properties of **1**-**4.**

Compd	$E_{ox}^{1/2}$ (V)[a]	E_{ox}^{onset} (V)[a]	E_{ox} (V)[a]	HOMO (eV)	LUMO (eV)	E_g[c] (eV)
1	0.64	0.56	0.77	-5.36[a] / -4.68[b]	-2.38[c] / -1.03[b]	2.98[d] / 3.65[b]
2	0.66	0.59	0.74	-5.39 / -4.63	-2.68 / -1.55	2.71 / 3.07
3	0.42	0.33	0.51	-5.13 / -4.60	-2.51 / -1.61	2.62 / 2.99
4	0.47	0.37	0.58	-5.17 / -4.68	-2.98 / -2.31	2.19 / 2.37

[a] Determined by CV calculated by the empirical formulae $E_{HOMO} = -(4.8 - E_{ox}^{onset})$, [b] DFT (B3LYP/6-31G*) calculations. $E_{LUMO} = E_{HOMO} + E_g$, [c] LUMO = HOMO+$E_g$, [d] Estimated from UV-Vis absorption spectra.

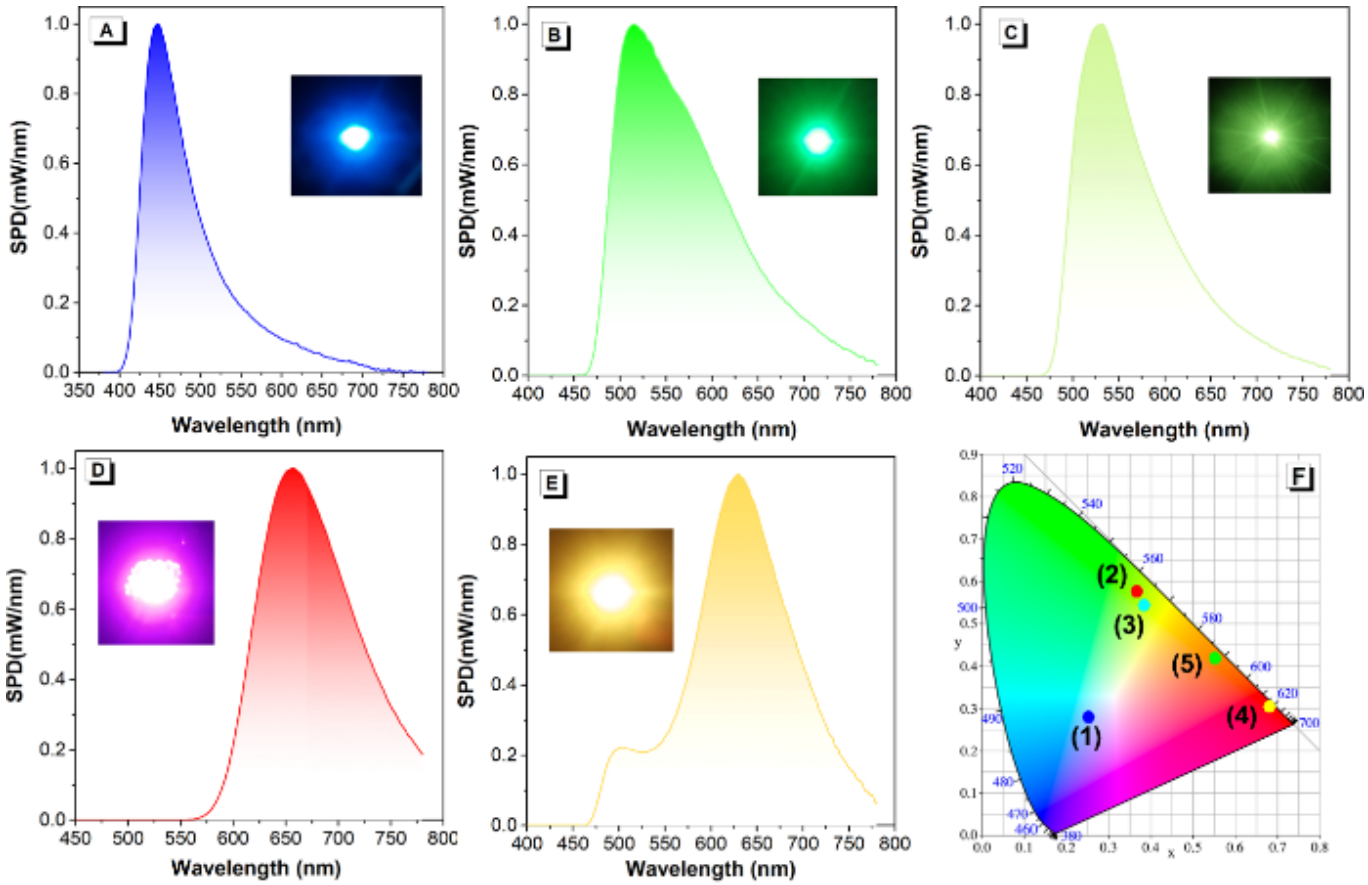

Fig. 6 The fluorescence spectra of (A) b-LED 1, (B) g-LED 2 (C) g- LED 3, (D) r- LED 4 and (E) y-LED 5 using compound **1**, compound **2**, compound **3**, compound **4** and a mixture of **1** and **4** as emitters, respectively. Insert: the photograph of the LEDs 1-5 with the emission centred at 447 nm, 507 nm, 524 nm, 656 nm and 629 nm, respectively. (F) CIE chromaticity coordinates of the blue, green, red and yellow LED device.

Table 3 The photoelectric parameters of the fabricated LED devices with under a drive current of 100 mA.

Devices	CCT (K)	CRI	R9	$\lambda_{max\ em}$	QY[a]	CIE (x, y)	Efficiency (lm/W)
b-LED 1	100000	70.1	-17	447	0.47	(0.25, 0.28)	0.02
g-LED 2	6324	21.1	-181	507	0.84	(0.39, 0.54)	2.5
g-LED 3	5904	11.9	-205	524	0.97	(0.34, 0.60)	6.9

r-LED 4	1280	23.1	-109	656	0.70	(0.69, 0.31)	2.9
y-LED 5[a]	1860	86.9	51	629	0.61	(0.55, 0.42)	0.8

[a] measured in doped film ($wt\%_{resin}$:$wt\%_{emitter}$ = 1:100).

spectrum in the range from 460 to 780 nm. The LED devices exhibited a high CRI of 86.7, CIE at (0.55, 0.42). The low luminous efficacy (0.8 lm/W) of these LED devices may be attributed to the relatively insufficient emission intensity of blue emitter **1**. All in all, the compounds **1**-**4** are excellent tunable-emission materials for LED applications (Table 3).

Recently, with the development of the microelectronics technology, personalized intelligent lighting and lighting control systems have been widely utilized in smart houses/buildings to save energy, facilitate people's lives, as well as decorate our community environment.[32] The tunable-emission materials with multi-color LED devices offer an application possibility for personalized intelligent lighting. Therefore, we further constructed an efficient electro circuit system to realize voice-activated intelligent lighting (Figs. S19 and S20), where the intelligent lighting modules involve a sound sensor module, power module, crystal oscillator module, reset module and the pre-fabricated LED devices with red, green, and yellow light (Fig. 7). For example, when the voice command is “red on or green on or yellow on”, the corresponding LED device can be lit, respectively, and the LED device can also be closed by voice control methods. Further studies on this intelligent lighting system and programs are ongoing in our lab to improve the response time and multi-scene applications (Movie S1).

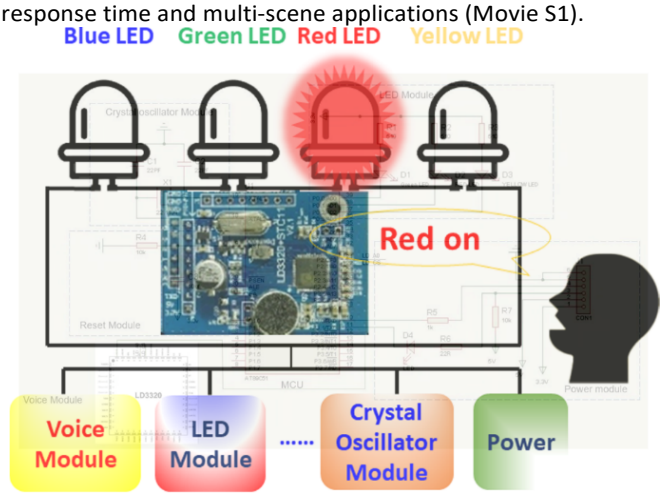

Fig. 7 The schematic diagram of designed intelligent lighting and lighting control system.

Conclusions

In summary, this article presents a simple pull-push system by using electron-donating units, and incorporating a suitable electron-withdrawing (A) group such as phenyl, pyrenyl with the benzothiadiazole unit, where the energy gap of the organic luminescent molecules were well adjusted, and we accessed color-tunable emission materials from blue (449 nm) to red light (661 nm). This series of thermally stable organic molecules with excellent color-tunable emission properties have been used for the preparation of high-performance RGB LED devices. Furthermore, the prepared LED devices were turned on and off by voice-activated controlled via microelectronics technology. This work demonstrates a new possible route to realizing the simple RGB organic luminescent materials for potential applications in smart house/city by combining organic synthesis, optoelectronic devices and microelectronic technologies.

Experimental section

Materials

Unless otherwise stated, all reagents used were purchased from commercial sources and were used without further purification. The 7-*tert*-butyl-1,3,5,9-tetrakisbromopyrene was prepared according to a previous report.[33] Epoxy resin (A) and curing agent (B) was purchased from Shenzhen Looking Long Technology co. LTD.

Characterization

^{1}H and ^{13}C NMR spectra were recorded on a Bruker AVANCE III 400M spectrometer using the DMSO-d_6 (or d-$CDCl_3$) as solvent (DMSO, ^{1}H: δ = 2.50 ppm, ^{13}C: δ = 39.5 ppm), Coupling constants (J) values are given in hertz (Hz). High-resolution mass spectra (HRMS) were taken on a LC/MS/MS, which consisted of a HPLC system (Ultimate 3000 RSLC, Thermo Scientific, USA) and a Q Exactive Orbitrap mass spectrometer. UV-vis absorption spectra and Photoluminescence (PL) spectra were recorded on a Shimadzu UV-2600 and a Hitachi F-4700 fluorescence spectrometer. PL quantum yields were measured using absolute methods using a Hamamatsu C11347-11 Quantaurus-QY Analyzer. The cyclic voltammetry was carried out in 0.12 M tetrabutylammonium hexafluorophosphate in anhydrous dichloromethane and THF at a scan rate of 100 $mV{\cdot}s^{-1}$ at room temperature. Thermogravimetric analysis was carried on a TA TGA Q5500 under dry nitrogen at a heating rate of 10 °C/min. Thermal transitions were investigated by differential scanning calorimetry using a TA DSC Q1000 under dry nitrogen at a heating rate of 10 °C/min. The quantum chemistry calculations were performed using the Gaussian 09W (RB3LYP/6-311G(d,p) basis set) software package.[34]

X-ray Crystallography

Crystallographic data for compound **4** was collected on a Bruker APEX 2 CCD diffractometer with graphite monochromated Mo Kα radiation (λ = 0.71073 Å) in the ω scan mode.[35, 36] The structure was solved by charge flipping or direct methods algorithms and refined by full-matrix least-squares methods on F^2.[37-39] Further details are provided in Table S1 . CCDC 2119848 contain the supplementary crystallographic data for this paper. These data can be obtained free of charge from The Cambridge

Crystallographic Data Centre via www.ccdc.cam.ac.uk/structures.

Synthesis

Synthesis of $N^4,N^4,N^{4''},N^{4''}$-tetrakis (4-methoxyphenyl)-[1,1':4',1''-terphenyl]-4,4''-diamine (1)

A mixture of 1,4-dibromobenzene (135 mg, 0.58 mmol, 1.0 eq.), (4-(bis(4-methoxyphenyl)amino)phenyl)boronic acid (474 mg, 1.36 mmol, 2.3 eq.) and K_2CO_3 (300 mg, 2.17 mmol, 3.7 eq.) were dissolved in toluene (10 mL), ethanol (2 mL) and water (2 mL) at room temperature for 10 mins under an argon atmosphere, then $Pd(PPh_3)_4$ (90 mg, 0.08 mmol, 0.1 eq.) was added. The resulting mixture was heated to 90 °C with stirring for 24 h. After it was cooled, the reaction mixture was poured into water (50 mL) and extracted with CH_2Cl_2 (2 ×50 mL). The organic layer was washed with water (2 × 40 mL) and saturated brine (50 mL), and then the solution was dried ($MgSO_4$) and condensed under reduced pressure. The residue was purified by column chromatography eluting with CH_2Cl_2-hexane (1:1) to give $N^4,N^4,N^{4''},N^{4''}$-tetrakis(4-methoxyphenyl)-[1,1':4',1''-terphenyl]-4,4''-diamine (**1**) (257 mg, 67%) as a light blue solid. ^{1}H NMR (400 MHz, DMSO-d_6, δ): δ 7.62 (s, 4H), 7.52 (d, J = 8.6 Hz, 4H), 7.05 (d, J = 8.8 Hz, 8H), 6.92 (d, J = 8.7 Hz, 8H), 6.84 (d, J = 8.6 Hz, 4H), 3.75 (s, 12H, OCH_3) ppm. ^{13}C NMR (101 MHz, d-DMSO) δ: ^{13}C NMR (101 MHz, DMSO) δ 156.2, 148.3, 140.5, 138.3, 131.6, 127.5, 127.1, 126.7, 120.1, 115.4, 55.7 ppm. HRMS (FTMS+p APCI) m/z: $[M+H]^+$ calcd for $C_{46}H_{40}N_2O_4$, 685.2988; found, 685.3060.

Synthesis of 4,4',4'',4'''-(7-(*tert*-butyl) pyrene-1,3,5,9-tetrayl)tetrakis(*N*,*N*-bis(4-methoxyphenyl)aniline) (2)

A mixture of 1,3,5,9-tetrabromo-7-(*tert*-butyl)pyrene (156 mg, 0.27 mmol, 1.0 eq.), (4-(bis(4-methoxyphenyl)amino) phenyl)boronic acid (506 mg, 1.45 mmol, 5.4 eq.) and K_2CO_3 (300 mg, 2.17 mmol, 8.0 eq.) were dissolved in toluene (10 mL), ethanol (2 mL) and water (2 mL) at room temperature for 10 mins under an argon atmosphere, then Pd $(PPh_3)_4$ (90 mg, 0.08 mmol, 0.1 eq.) was added. The resulting mixture was heated to 90 °C with stirring for 24 h. After it was cooled, the reaction mixture was poured into water (50 mL) and extracted with CH_2Cl_2 (2 ×50 mL). The organic layer was washed with water (2 × 40 mL) and saturated brine (50 mL), and then the solution was dried ($MgSO_4$) and condensed under reduced pressure. The residue was purified by column chromatography eluting with CH_2Cl_2-hexane (2:1) to give 4,4',4'',4'''-(7-(*tert*-butyl)pyrene-1,3,5,9-tetrayl)tetrakis(*N*,*N*-bis(4-methoxyphenyl)aniline) (**2**) (160 mg, 40%) as a light yellow green solid. ^{1}H NMR (400 MHz, DMSO-d_6, δ) : 8.33 (s, 2H, Pyrene H), 8.09 (s, 2H, Pyrene H), 7.81 (s, 1H, Pyrene H), 7.42 (dd, *J* = 17.5, 7.8 Hz, 8H, Ar H), 7.08 (t, *J* = 8.8 Hz, 16H, Ar H), 6.88 (t, *J* = 9.1 Hz, 24H, Ar H), 3.71 (d, *J* = 6.1 Hz, 24H, OCH_3), 1.35 (s, 9H, *t*Bu H) ppm. HRMS (FTMS+p APCI) m/z: $[M+H]^+$ calcd for $C_{100}H_{86}N_4O_8$, 1472.7748; found, 1472.6554.

Synthesis of 4,4',4'',4'''-(pyrene-1,3,6,8-tetrayl) tetrakis (*N*,*N*-bis(4-methoxyphenyl)aniline) (3)

A mixture of 1,3,6,8-tetrabromo-pyrene (200 mg, 0.35 mmol, 1.0 eq.), (4-(bis(4-methoxyphenyl)amino)phenyl)boronic acid (608 mg, 1.74 mmol, 5.0 eq.) and K_2CO_3 (300 mg, 2.17 mmol, 8.0 eq.) were dissolved in toluene (10 mL), ethanol (2 mL) and water (2 mL) at room temperature for 10 mins under an argon atmosphere, then Pd $(PPh_3)_4$ (90 mg, 0.08 mmol, 0.1 eq.) was added. The resulting mixture was heated to 90 °C with stirring for 24 h. After it was cooled, the reaction mixture was poured into water (50 mL) and extracted with CH_2Cl_2 (2 ×50 mL). The organic layer was washed with water (2 × 40 mL) and saturated brine (50 mL), and then the solution was dried ($MgSO_4$) and condensed under reduced pressure. The residue was purified by column chromatography eluting with CH_2Cl_2-hexane (3:1) to give 4,4',4'',4'''-(7-(*tert*-butyl)pyrene-1,3,5,9-tetrayl)tetrakis(*N*,*N*-bis(4-methoxyphenyl)aniline) (**3**) (310 mg, 63%) as a yellow solid. ^{1}H NMR (400 MHz, DMSO-d_6, δ) δ: 8.19 (s, 4H, Pyrene H), 7.90 (s, 2H, Pyrene H), 7.49 (d, *J* = 7.4 Hz, 8H, Ar H), 7.14 (d, *J* = 8.1 Hz, 16H, Ar H), 6.95 (t, *J* = 7.6 Hz, 24H, Ar H), 3.76 (s, 24H, OCH_3) ppm. HRMS (FTMS+p APCI) m/z: $[M+H]^+$ calcd for $C_{96}H_{78}N_4O_8$; 1416.6685; found, 1416.5935.

Synthesis of 4,4'-(benzo[c][1,2,5]thiadiazole-4,7-diyl) bis(*N*,*N*-bis(4-methoxyphenyl)aniline) (4)

A mixture of 4,7-dibromo-2,1,3-benzothiadiazole (150 mg, 0.51 mmol, 1 eq.), (4-(bis(4-methoxyphenyl)amino) phenyl)boronic acid (450 mg, 1.28 mmol, 2.5 eq.) and K_2CO_3 (300 mg, 2.17 mmol, 4.3 eq.) were dissolved in THF (10 mL) at room temperature for 10 mins under an argon atmosphere, then Pd $(PPh_3)_4$ (60 mg, 0.05 mmol, 0.1 eq.) was added. The resulting mixture was heated to 90 °C with stirring for 24 h. After it was cooled, the reaction mixture was poured into water (50 mL) and extracted with CH_2Cl_2 (2 ×50 mL). The organic layer was washed with water (2 × 40 mL) and saturated brine (50 mL), and then the solution was dried ($MgSO_4$) and condensed under reduced pressure. The residue was purified by column chromatography eluting with CH_2Cl_2-hexane (2:1) to give 4,4'-(benzo[c][1,2,5]thiadiazole-4,7-diyl)bis(*N*,*N*-bis(4-methoxyphenyl)aniline) (**4**) (170 mg, 45%) is a red colored solid. ^{1}H NMR (400 MHz, DMSO-d_6, δ): 7.86 (d, *J* = 8.8 Hz, 4H, Ar H), 7.81 (s, 2H), 7.23 – 7.03 (m, 8H, Ar H), 7.03 – 6.93 (m, 8H, Ar H), 6.89 (d, *J* = 8.8 Hz, 4H, Ar H), 3.76 (s, 12H, OCH_3) ppm. ^{13}C NMR (151 MHz, d-$CDCl_3$) δ 156.3, 154.3, 132.0, 129.6, 127.2, 123.7, 119.9, 114.7, 100.0, 55.52 ppm. HRMS (FTMS+p APCI) m/z: $[M+H]^+$; calcd for $C_{46}H_{38}N_4O_4S$, 743.2614; found, 743.2683.

Fabrication of LED[40]

In the packaging procedure, for LED **1**-**4**, 1 mg of compound **1**-**4** powder (for LED **5**: a mixture of compound **1** (0.3 mg) and compound **4** (0.7 mg) in 100 mg resin) was mixed with 100 mg resin (A:B = 1:1 in weight), respectively. The resulting mixture was vacuumed for 0.5 h to remove the bubbles. After that, the mixture was dropped onto a certain chip and thermally cured at 100 °C for 2 h in an oven. The prepared on-chip LED device was eventually obtained and the detailed information is summarized in the table below.

Table 4 The fabricated LED devices using compounds **1**-**4**

Devices	Chip type	λ_{ex} (nm)	Device emission Color
b-LED 1	*InGaN*	365	blue
g-LED 2	*InGaN*	365	green
g-LED 3	*InGaN*	365	green
r-LED 4	*InGaN*	450	red
y-LED 5	*InGaN*	365	yellow

Author Contributions

Y. Liu, X. Wang, H. Zhu and J. Zhang performed investigation, Y. Wang performed the LED devices and test, X. Song and D. Wang performed the voice-activated intelligent lighting system, J. Bai measured the single crystal X-ray diffraction, C. Redshaw contribution in revising the manuscript and giving scientific advice. X.-L. Ni carried out DFT calculation. X. Feng and B. Z. Tang contribution in designing and supervising the whole project.

Conflicts of interest

The authors have no conflict of interest to declare.

Acknowledgements

Y. Liu, Y. Wang and X. Song contributed equally to this work. This work was supported by the National Natural Science Foundation of China (21975054), Natural Science Foundation of Guangdong Province of China (2019A1515010925), Guangdong Provincial Key Laboratory of Information Photonics Technology (2020B121201011), "One Hundred Talents Program" of the Guangdong University of Technology (GDUT) (1108-220413205), Science and Technology Planning Project of Hunan Province (2018TP1017), the Open Fund of Guangdong Provincial Key Laboratory of Luminescence from Molecular Aggregates, Guangzhou 510640, China (South China University of Technology) (2019B030301003), Science and Technology Planning Project of Hunan Province (2018TP1017), CR thanks the EPSRC for an Overseas Travel Grant (EP/R023816/1). The information of LEDs were supported by Shenzhen Looking Long Technology co., LTD.

References

1 Z. Lv, J. Lloret, H. Song, J. N. de Souza and C. X. Mavromoustakis, *IEEE Netw.*, 2021, **35**, 16-17.
2 L. M. Gladence, V. M. Anu, R. Rathna and E. Brumancia, *J Ambient. Intell. Humaniz. Comput.*, 2020, DOI: 10.1007/s12652-020-01968-2.
3 J. F. De Paz, J. Bajo, S. Rodríguez, G. Villarrubia and J. M. Corchado, *Inf. Sci.*, 2016, **372**, 241-255.
4 W. T. Xu, J. Zhang, J. Y. Kim, W. Huang, S. S. Kanhere, S. K. Jha and W. Hu, *IEEE Internet Things J.*, 2019, **6**, 7266-7281.
5 A. M. Yang, C. Y. Zhang, Y. J. Chen, Y. X. Zhuansun and H. X. Liu, *IEEE Internet Things J.*, 2020, **7**, 2521-2530.
6 X. Zhang, S. Liu, L. Zhang and W. Xie, *Adv. Opt. Mater.*, 2018, **7**, 1800857.
7 G. Tan, S. Chen, C.-H. Siu, A. Langlois, Y. Qiu, H. Fan, C.-L. Ho, P. D. Harvey, Y. H. Lo, L. Liu and W.-Y. Wong, *J. Mater. Chem. C*, 2016, **4**, 6016-6026.
8 A. S. Klymchenko, *Acc. Chem. Res.*, 2017, **50**, 366-375.
9 W. Mao, J. Tang, L. Dai, X. He, J. Li, L. Cai, P. Liao, R. Jiang, J. Zhou and H. Wu, *Angew. Chem. Int. Ed.*, 2021, **60**, 2393-2397.
10 Q. Wang, Q. Zhang, Q. W. Zhang, X. Li, C. X. Zhao, T. Y. Xu, D. H. Qu and H. Tian, *Nat. Commun.*, 2020, **11**, 158.
11 Z. Cui, A. Abdurahman, X. Ai and F. Li, *CCS Chem.*, 2020, **2**, 1129-1145.
12 J. P. Mora-Fuentes, I. Papadopoulos, D. Thiel, R. Alvarez-Boto, D. Cortizo-Lacalle, T. Clark, M. Melle-Franco, D. M. Guldi and A. Mateo-Alonso, *Angew. Chem. Int. Ed. Engl.*, 2020, **59**, 1113-1117.
13 Z. Wu, J. Nitsch, J. Schuster, A. Friedrich, K. Edkins, M. Loebnitz, F. Dinkelbach, V. Stepanenko, F. Wurthner, C. M. Marian, L. Ji and T. B. Marder, *Angew. Chem. Int. Ed. Engl.*, 2020, **59**, 17137-17144.
14 X. Deng, X. Yu, J. Xiao and Q. Zhang, *Aggregate*, 2021, **2**, e35.
15 L. Zhang, L. Yi, Z. J. Sun and H. X. Deng, *Aggregate*, 2021, **2**, e24.
16 S. Wu, H. Min, W. Shi and P. Cheng, *Adv. Mater.*, 2020, **32**, e1805871.
17 B. Xu, H. Wu, J. Chen, Z. Yang, Z. Yang, Y. C. Wu, Y. Zhang, C. Jin, P. Y. Lu, Z. Chi, S. Liu, J. Xu and M. Aldred, *Chem. Sci.*, 2017, **8**, 1909-1914.
18 X. Ma, L. Jia, B. Z. Yang, J. P. Li, W. Huang, D. Y. Wu and W. Y. Wong, *J. Mater. Chem. C*, 2021, **9**, 727-735.
19 C. S. Li, R. S. Nobuyasu, Y. K. Wang, F. B. Dias, Z. J. Ren, M. R. Bryce and S. K. Yan, *Adv. Opt. Mater.*, 2017, **5**, 1700435.
20 J. Wang, F. Tang, Y. Wang, S. Liu and L. Li, *Adv. Opt. Mater.*, 2020, **8**, 1901571.
21 Z. L. Xie, Q. Y. Huang, T. Yu, L. Y. Wang, Z. Mao, W. L. Li, Z. Yang, Y. Zhang, S. W. Liu, J. R. Xu, Z. G. Chi and M. P. Aldred, *Adv. Funct. Mater.*, 2017, **27**, 1703918.
22 C. Liu, H. Bai, B. He, X. He, J. Zhang, C. Chen, Y. Qiu, R. Hu, F. Zhao, Y. Zhang, W. He, J. H. C. Chau, S. Chen, J. W. Y. Lam and B. Z. Tang, *Angew. Chem. Int. Ed.*, 2021, **60**, 12424-12430.
23 Q. Wang, W. Gao, Y. Chen, X. Wang, J. Zeng, Y. Liu, H. Ran, Z. Hu, J. Bai, X. Feng, C. Redshaw, Q. Chen and J. Y. Hu, *Asian J. Org. Chem.*, 2020, **10**, 233-240.
24 X. Mao, F. Xie, X. Wang, Q. Wang, Z. Qiu, M. R. J. Elsegood, J. Bai, X. Feng, C. Redshaw, Y. Huo, J. Y. Hu and Q. Chen, *Chin. J. Chem .* 2021, **39**, 2154-2162.
25 X. H. Wang, L. R. Wang, X. Y. Mao, Q. S. Wang, Z. F. Mu, L. An, W. Zhang, X. Feng, C. Redshaw, C. Y. Cao, A. J. Qin and B. Z. Tang, *J. Mater. Chem. C*, 2021, **9**, 12828-12838.
26 A. G. Crawford, A. D. Dwyer, Z. Liu, A. Steffen, A. Beeby, L.-O. Pålsson, D. J. Tozer and T. B. Marder, *J. Am. Chem. Soc.*, 2011, **133**, 13349-13362.
27 H. B. Wang, J. N. Huo, H. B. Tong, X. H. Wei, Y. Zhang, Y. B. Li, S. M. Chen, H. P. Shi and B. Z. Tang, *J. Mater. Chem. C*, 2020, **8**, 14208-14218.
28 X. Feng, J. Y. Hu, C. Redshaw and T. Yamato, *Chem. Eur. J.*, 2016, **22**, 11898-11916.
29 Q. Li and Z. Li, *Acc. Chem. Res.*, 2020, **53**, 962-973.
30 Z. Zhang, H. Bi, Y. Zhang, D. Yao, H. Gao, Y. Fan, H. Zhang, Y. Wang, Y. Wang, Z. Chen and D. Ma, *Inorg. Chem.*, 2009, **48**, 7230-7236.
31 Y. Zhan, L. Lin, M. Chen and L. Wu, *ACS Appl. Mater. Interfaces*, 2018, **10**, 33390-33398.
32 F. X. Wang, J. C. Liu, C. Zhang, L. F. Sun and K. Hwang, *IEEE Netw.*, 2021, **35**, 170-176.
33 X. Feng, J. Y. Hu, F. Iwanaga, N. Seto, C. Redshaw, M. R. Elsegood and T. Yamato, *Org. Lett.*, 2013, **15**, 1318-1321.
34 G. M.J.T. Frisch, Gaussian 09, revision A. 02, Gaussian, Inc., Pittsburgh, PA, 2009., Gaussian.
35 Frisch, m. J. Et al. Gaussian 03, revision c.02, gaussian, inc., wallingford, ct, 2004.
36 Saint and apex 2. Software for ccd diffractometers. 2015.
37 G. M. Sheldrick, *Acta Crystallogr. Sect. A: Found. Crystallogr.*, 2015, **71**, 3-8.
38 S. P. Westrip, *J. Appl. Crystallogr.*, 2010, **43**, 920-925.
39 J. Zhang, X. F. Ma and X. P. Xuan, *Chin. J. Struct. Chem.*, 2020, **39**, 698-708.
40 S. Yuan, Z. K. Wang, L. X. Xiao, C. F. Zhang, S. Y. Yang, B. B. Chen, H. T. Ge, Q. S. Tian, Y. Jin and L. S. Liao, *Adv. Mater.*, 2019, **31**, e1904319.

